Quantum contextuality of complementary photon polarizations explored by adaptive input state control

Kengo Matsuyama,[*] Ming Ji,[†] Holger F. Hofmann,[‡] and Masataka Iinuma[§]
Graduate School of Advanced Science and Engineering, Hiroshima University, 1-3-1 Kagamiyama, Higashi-Hiroshima 739-8530, Japan

(Received 11 July 2023; accepted 22 November 2023; published 15 December 2023)

We experimentally investigate nonlocal contextual relations between complementary photon polarizations by adapting the entanglement and the local polarizations of a two-photon state to satisfy three deterministic conditions demonstrating both quantum contextuality and nonlocality. The key component of this adaptive input state control is the variable degree of entanglement of the photon-pair source. Local polarization rotations can optimize two of the three correlations, and the variation of the entanglement optimizes the third correlation. Our results demonstrate that quantum contextuality is based on a nontrivial trade-off between local complementarity and quantum correlations.

DOI: 10.1103/PhysRevA.108.062213

I. INTRODUCTION

Although it seems natural to assume that the values of a physical property are independent of the way in which they are measured, the Bell-Kochen-Specker theorem proves that this assumption cannot be reconciled with the predictions of quantum theory [1–14]. The theoretical predictions of the Bell-Kochen-Specker theorem have been demonstrated in many experiments, including the well-known experimental observation of Bell's inequality violations [15–37]. It has been argued that Bell's inequalities are not optimal for the demonstration of nonlocality and contextuality because they involve a nontrivial statistical limit. Instead, it may be better to define contextuality in terms of logically necessary conclusions that are then violated with nonvanishing probability or even with certainty in specific quantum systems. The most notable examples of such proofs of nonlocality without inequalities are the Greenberger-Horne-Zeilinger (GHZ) paradox [38,39] and Hardy's paradox [40,41], both of which have been confirmed in various experiments [39,42–45]. All of these scenarios indicate that contextuality is a fundamental feature of the nonclassical relation between different physical properties. However, the initial quantum state used in these experiments is not defined in terms of its physical properties. Instead, the measurements made to verify the paradox are adapted to the specific quantum coherence of the available input state. Since the initial assumption of perfect quantum coherence makes it difficult to understand how imperfections in quantum-state preparation appear in the experimentally observed statistics, it may be useful to introduce an operational definition of state preparation that defines the intended state in terms of a desired set of measurement outcomes. Such an operational definition of the input state can be formulated as an optimization problem that is independent of experimental imperfections. The merits of this kind of approach have already been recognized in the optimization of Bell's inequality violations intended to close the various loopholes caused by experimental imperfections [22,24–27,30]. In particular, it was found that the experimentally observed violation of a Bell's inequality can be improved by using a source that initially generates a pure state with nonmaximal entanglement [46]. However, these methods of state adaption are usually targeted at specific error syndromes that break the symmetry of the original scenario, requiring an adjustment of the state that would not be needed in the ideal limit. Here, we focus on a scenario that has no intrinsic symmetry, so that the ideal source already defines a specific set of preferred polarization directions. It is then possible to formulate an operational procedure that optimizes the essential statistical features observed in this scenario even in the limit of very small experimental imperfections. This procedure thus highlights the essential features of quantum contextuality, independent of the precise nature of these imperfections. We can thus develop a better practical understanding of the role of complementary photon polarizations in the observation of quantum contextuality.

In the present paper, we explore the possibility of modifying the input state to fit a specific set of statements that define a contextuality paradox. For this purpose, we first identify the physical properties and their desired relations and then modify the state preparation process until it optimally satisfies the conditions set by these relations. We thus define the initial state entirely in terms of its observable properties, providing a complete operational definition of the physics of state preparation. Our approach has been inspired by the Gedankenexperiment of Frauchiger and Renner [47], where an entangled state is defined in terms of an interaction intended to provide information about a specific local observable of one of the two systems, and the initial experimental realization of the paradox was achieved by interacting separate input photons using linear optics and postselection [48]. This experimental work also showed that the expression of the paradox as an inequality violation is equivalent to a standard Bell's inequality, where no special considerations

[*]matsuyama@huhep.org
[†]d215181@hiroshima-u.ac.jp
[‡]hofmann@hiroshima-u.ac.jp
[§]iinuma@hiroshima-u.ac.jp

need to be given to the precise conditions set forth in the formulation of the paradox. As pointed out in the paper, the essential difference between contextuality and nonlocality arise from the choice of conditions that are discussed [48]. In the following, we formulate the paradox in the form of contradictions between statements observed in separate measurements without invoking any conditions of locality. However, we replace the interactions in the original protocol with a more efficient quantum-state preparation process that can be adapted by varying the entanglement generated and the local polarization directions. Different from Hardy's paradox, we require that the pairs of polarization orientations used to formulate the paradox are always complementary, setting a condition under which the statistics of the input state can be optimized. As we have pointed out in previous work [49], the characteristic correlations of the paradox discussed by Frauchiger and Renner uniquely define the initial quantum state in terms of measurement probabilities of zero observed for specific combinations of local outcomes. It is therefore possible to operationally define the state preparation process as a simultaneous suppression of specific outcomes in different measurement contexts. Here, we realize this adaptive state preparation process for polarization entangled photon pairs using a nonlinear crystal from both sides with two-separated pump beams inside of a Sagnac interferometer [50–53]. This setup allows us to control the degree of entanglement by changing the pump beam polarization, completely preserving the two-photon coherence in the output at all settings. In addition to the degree of entanglement, the local polarization of each photon can be rotated, providing us with three adjustable parameters in the state preparation process.

As shown in the following, it is possible to suppress two of the three outcome probabilities by optimizing only the local polarization rotations. Since the suppression of these probabilities is due to the destructive interference between two output components, the optimal suppression can be found by identifying the local polarization rotation with equal measurement probabilities for the two interfering components. Our results show that this method of outcome suppression is highly efficient, allowing us to optimize the local polarization rotations for a fixed degree of entanglement. The third outcome probability then depends on the initial degree of entanglement. It is possible to achieve optimal suppression of this probability by varying the degree of entanglement. It should be emphasized that this method of adaptive state control optimizes the state preparation process based on the observed measurement outcomes and requires no further assumptions regarding the quality of the down-conversion source. This approach has three distinct advantages, (a) the optimization of parameters partially compensates the effects of experimental imperfections, improving the performance of noisy sources, (b) quantum state preparation is directly related to the specific correlations relevant for the observation of the contextuality paradox, and (c) the optimization of quantum interference effects can be realized by observing the output probabilities of the components that interfere with each other, providing a practical illustration of complementarity in quantum state preparation.

The goal of adaptive input state control is the optimization of the contextuality paradox associated with the nonzero probability of a specific measurement outcome observed after the three state preparation conditions have been satisfied. We can therefore evaluate the success of the procedure using a contrast function K that relates the residual probabilities of the three outcomes suppressed in adaptive input state control to the nonzero probability that characterizes the paradox. In the present experimental setup, we achieve a contrast of about 0.5 over a wide range of settings controlling the degree of entanglement. The observation of quantum contextuality is thus found to be very robust against changes in the available amount of entanglement. Another interesting aspect of the results is that the maximal contrast K is observed for a degree of entanglement corresponding to an equal balance of local polarization and entanglement. The conditions for the observation of quantum contextuality involve both local and nonlocal aspects of quantum statistics, possibly revealing new aspects of the relation between local complementarity and entanglement that are hidden by the abstract representation of the initial state as a superposition of specific basis states.

The rest of the paper is organized as follows: Section II describes the contextuality paradox and the manner in which it defines adaptive state control. Section III describes the experimental setup and its characteristic properties. Section IV describes the adaptive state control and the experimental results obtained from it. Section V evaluates the successful observation of quantum contextuality in terms of the contrast K. Section VI concludes the paper.

II. OPTIMIZATION OF QUANTUM CONTEXTUALITY BY ADAPTIVE INPUT STATE CONTROL

The Gedankenexperiment proposed by Frauchiger and Renner is intended to show that the predictions of quantum mechanics are not consistent with each other [47]. In the original Gedankenexperiment, two observers make statements about the outcomes observed by the other party based on their own results. It is then shown that a set of statements that seemingly contradict each other can all be valid with a certainty of one hundred percent. As we pointed out in our previous paper [49], the requirement of maximal certainty uniquely determines a specific initial state. It is therefore natural to conclude that the paradox itself provides an operational definition of a quantum state.

We are considering a situation where two separate physical systems satisfy three statements that can be represented by probabilities of zero for three measurement outcomes obtained in different contexts represented by the local measurements of F_1, F_2 and W_1, W_2, respectively [49],

$$P(F_1 = 0, W_2 = a) = 0, \tag{1}$$

$$P(W_1 = a, F_2 = 0) = 0, \tag{2}$$

$$P(F_1 = 1, F_2 = 1) = 0, \tag{3}$$

where the property F_1, F_2 is either 0 or 1 and the property W_1, W_2 is either a or b. Equations (1) and (2) ensure that if the outcome for one system is $W_i = a$, the other system will always show an outcome of $F_j = 1$. It would thus be natural to conclude that the outcome $W_1 = W_2 = a$ requires that $F_1 = F_2 = 1$, even if no data on F_1, F_2 are available. Since Eq. (3) states that a simultaneous detection of $F_j = 1$

in both systems is impossible, noncontextual logic suggests that an outcome of $W_1 = W_2 = a$ for the two systems should also be impossible. Since it appears that $W_1 = W_2 = a$ is only possible if at least one of the outcomes in Eqs. (1)–(3) can be observed as well, $P(W_1 = a, W_2 = a)$ should not be greater than the sum of the probabilities in Eqs. (1)–(3). This relation among the four probabilities is given by

$$P(a, a) \leqslant P(0, a) + P(a, 0) + P(1, 1), \tag{4}$$

where $P(x, y)$ represents a joint probability with x as the outcome of F_1 or W_1 and y as the outcome of F_2 or W_2. It may be worth noting that this inequality is mathematically equivalent to a Bell's inequality [48], although here we use it to probe the consistency of different measurement contexts.

As pointed out in Ref. [49], the three conditions given above correspond to orthogonality relations in the Hilbert-space formalism. To satisfy all three conditions, a quantum state $|\psi\rangle$ must be orthogonal to the quantum states representing the measurement outcomes of $\hat{W}_i$ and $\hat{F}_i$,

$$\langle 0, a|\psi\rangle = 0, \tag{5}$$

$$\langle a, 0|\psi\rangle = 0, \tag{6}$$

$$\langle 1, 1|\psi\rangle = 0. \tag{7}$$

In the following, the operators $\hat{W}_i$ and $\hat{F}_i$ represent complementary polarization components. This means that the measurement outcomes 0,1 and a, b are mutually unbiased,

$$|a\rangle = \frac{1}{\sqrt{2}}(|0\rangle - |1\rangle), \tag{8}$$

$$|b\rangle = \frac{1}{\sqrt{2}}(|0\rangle + |1\rangle). \tag{9}$$

Equations (5)–(7) uniquely determine the quantum state $|\psi\rangle$, resulting in a probability of $P(a, a) = 1/12$ [47,49]. This is a specific version of Hardy's paradox [40,41], confirming both quantum contextuality and quantum nonlocality. However, the present formulation emphasizes the fact that the initial quantum state is fully defined by experimentally observable conditions given by Eqs. (1)–(3). As shown in Ref. [49], realizing these conditions will necessarily result in a nonzero probability for the outcome $W_1 = W_2 = a$. We can therefore develop a method of state preparation that optimizes these conditions in the presence of arbitrary experimental imperfections.

Since the state defined by the conditions in Eqs. (5)–(7) is a partially entangled state, it is necessary to vary the available degree of entanglement. In quantum optics, photon pairs with variable degrees of polarization entanglement can be generated efficiently by parametric down-conversion in a Sagnac interferometer [50–53]. Since the polarizations of the photons generated in the down-conversion are initially aligned with the optical axes of the nonlinear crystal, the initial quantum state is given by

$$|\psi_0\rangle = \cos\phi_S|H, H\rangle - \sin\phi_S|V, V\rangle, \tag{10}$$

where the ϕ_S is an experimentally adjustable parameter that controls the degree of entanglement. Any pure state with this degree of entanglement can now be obtained by local polarization rotations. Due to the symmetry of the conditions, we can apply the same polarization rotation ϕ_M to both photons, defining the states $|0\rangle$ and $|1\rangle$ as

$$|0\rangle = \hat{U}(\phi_M)|H\rangle, \quad |1\rangle = \hat{U}(\phi_M)|V\rangle. \tag{11}$$

Adaptive input state control requires that the rotation angle ϕ_M is adjusted to optimally satisfy the conditions (5) and (6) given by $P(0, a) = 0$ and $P(a, 0) = 0$. Experimentally, this procedure can be simplified by making use of Eq. (8). The conditions for the quantum state then read

$$\langle 0, 1|\psi\rangle = \langle 0, 0|\psi\rangle, \tag{12}$$

$$\langle 1, 0|\psi\rangle = \langle 0, 0|\psi\rangle. \tag{13}$$

Experimentally, the coherence is supplied by the initial state $|\psi_0\rangle$, so the optimal rotation angle ϕ_M can be found by satisfying the conditions $P(0, 0) = P(0, 1)$ and $P(0, 0) = P(1, 0)$. These conditions can always be satisfied exactly, independent of experimental imperfections. Once the local polarization rotations are determined, it is possible to evaluate the actual suppression of the probabilities $P(0, a)$ and $P(a, 0)$ by the corresponding measurements. In addition, the value of $P(1, 1)$ can be obtained for these local polarization rotations. The optimal suppression of $P(0, a)$ and $P(a, 0)$ results in a value of $P(1, 1)$ that depends on the parameter ϕ_S which is used to control the degree of entanglement. A suppression of $P(1, 1)$ thus requires an optimization of ϕ_S to adjust the amount of entanglement in the initial state.

It is interesting to note that only measurements in the $\{0, 1\}$ basis are needed for adaptive state control, even though the contextual statistics characterizes the relations between different combinations of $\{0, 1\}$ measurements and $\{a, b\}$ measurements. Adaptive state control thus highlights the manner in which the relations between different measurement contexts are defined by quantum coherence in the measurement outcomes [54].

III. EXPERIMENT

A. Experimental setup

As shown in Fig. 1, the experimental setup consists of a Sagnac-type interferometer used as the source of polarization entanglement, two polarization filters, and two single-photon detectors and electronics for signal processing. The pump laser (semiconductor laser, wavelength 405 nm) emits light through a fiber coupler (FC0). The polarization of the pump light can be controlled by the combination of a Glan-Taylor prism (GT0) and a half-wave plate (HWP0) to obtain polarizations from vertical (V) polarization to diagonal linear polarization (D). The pump beam enters the Sagnac interferometer indicated by a block-dotted box and is separated at a double polarization beam splitter (DPBS). The DPBS is custom made and works equally well at both 405 and 810 nm. It should be noted that this feature is not available in typical off-the-shelf products because the wavelength dependence of antireflection coatings limit the performance of most devices to a bandwidth that is much narrower than this wavelength difference.

In the clockwise path, the pump beam is converted from V polarization to H polarization by the double half-wave plate (DHWP). Both pump beams interact with the periodically

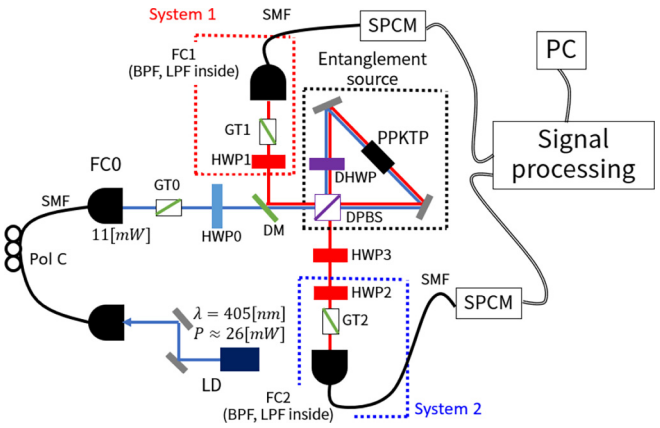

FIG. 1. Experimental setup for the adaptive input state control. The pump beam is a laser diode (LD) with a wavelength of 405 nm and its output power is 26 mW. A fiber coupler (FC0) emits the pump beam with power of 11 mW. The pump beam is separated at the double polarization beam splitter (DPBS) into two paths, pumping the periodically poled KTP crystal (1 mm × 1 mm × 10 mm) from both edges and creating photon pairs. A double half wave plate (DHWP) exchanges horizontal and vertical polarizations. The two paths then overlap at the DPBS and the photon pairs are separated there. The two photons are then detected separately by two single-photon counting modules (SPCM) after passing through polarization filters, bandpass filters (BPF) ($\lambda = 810$ nm, $\delta\lambda = 10$ nm), and long-pass filters (LPF) (transmission: $\lambda > 700$ nm). The detection setup for photon is shown inside the red-dotted box and the blue-dotted box. The output pulses were converted to NIM logic pulses of 30 ns and processed using a NIM logic circuit composed of logic level adapter, discriminator, and coincident counting module. The coincidence counts were recorded by a connected PC.

poled KTP (PPKTP) crystal to generate photon pairs with opposite HV polarizations. In the anticlockwise path, the DPBS separates the photons so that the V-polarized photons go leftward and the H-polarized photons go downward. In the clockwise path, the H-polarized photons go leftward and the V-polarized photons go downward. Since the photons from the clockwise path and the anticlockwise path are indistinguishable, the photon pairs in the output are polarization entangled. The leftward-directed photons are reflected by the dichroic mirror (DM) and measured in system 1 (indicated by the red-dotted box). The HV-polarization of the downward-directed photons is flipped from V to H and from H to V by HWP3 to prepare the symmetric quantum state given by Eq. (10). The downward-directed photons are then measured in system 2 (surrounded by the blue-dotted box). The photon pairs are measured using combinations of GT1, GT2 and HWP1, HWP2. Two bandpass filters (BPFs) and two long-pass filters (LPFs) inside two fiber couplers (FC1 and FC2) eliminate background photons and select photon pairs with $\lambda = 810$ nm. The photon pairs are detected by two single-photon counting modules (SPCMs), PerkinElmer (SPCM-AQR- 14-FC13237-1) and EXCELITAS (SPCM-AQRH-14-FC24360), and their coincidence counts are recorded in a computer.

In the present setup, the setting of HWP0 determined the control parameter ϕ_S. If the angle of the HWP0 is set so that the pump beam is V polarized, corresponding to $\phi_S = 0^\circ$, the pump beam passes through the clockwise path only, so that the output photon pairs results in the product state. If the angle of the HWP0 is set so that the pump beam is D-polarized, corresponding to $\phi_S = 45^\circ$, the photon pairs are in the maximally entangled state because the pump beam is divided with the almost same intensity into the clockwise and the anticlockwise paths. Continuously rotating the angle of the HWP0 should therefore provide us with full control over the degree of entanglement generated in the setup. The HWP1 and the HWP2 combine two distinct roles. One is to adjust the local polarization rotation ϕ_M, which is strictly speaking part of the state preparation, and the other is to switch the measured polarizations between $\{0, 1\}$ and $\{a, b\}$. Controlling both settings with only one HWP helps to reduce systematic errors. If the setup is modified for different applications, it may be necessary to perform these two functions using separate HWPs.

To characterize the performance of the entangled photon-pair source, we have evaluated the two-photon visibilities at $\phi_S = 45^\circ$. These visibilities can be given by the correlations

$$C_i \equiv \left| \frac{N_{++} + N_{--} - N_{+-} - N_{-+}}{N_{++} + N_{--} + N_{+-} + N_{-+}} \right|, \tag{14}$$

where $+$ and $-$ are the two possible outcomes for the respective polarization, N_{++} and N_{--} are the count rates for the same polarization, and N_{+-} and N_{-+} are the count rates for opposite polarizations. Evaluating each visibility for the HV and DA polarizations, the experimental results for our entanglement source are

$$C_{\mathrm{HV}} = 0.968 \pm 0.013, \tag{15}$$

$$C_{\mathrm{DA}} = 0.935 \pm 0.011. \tag{16}$$

Here, DA polarization refers to the diagonal and antidiagonal polarization directions. The visibility of the HV polarization is limited by imperfection of the wave plates and the polarizers. The main causes of limited visibility seem to be the HWP3, which is used to convert the positive correlation of the generated photon pairs into a negative correlation, and the DPBS with its extinction ratio of 10^2. In addition, the visibility of DA polarization is limited by the visibility of interference in the Sagnac interferometer. These experimental imperfections explain the reduced visibilities observed in the setup and given in Eqs. (15) and (16).

B. Entanglement witness and local polarizations

To evaluate the control of entanglement in our setup, we characterize the visibilities C_{HV} and C_{DA} for different settings of ϕ_S. The entanglement generated in the setup can then be evaluated by the entanglement witness given by

$$W_E \equiv C_{\mathrm{HV}} + C_{\mathrm{DA}} - 1. \tag{17}$$

Ideally, the reduction of entanglement results in an increase of the local polarization described by the visibility V_{HV}:

$$V_{\mathrm{HV}} = \frac{N_{\mathrm{H}} - N_{\mathrm{V}}}{N_{\mathrm{H}} + N_{\mathrm{V}}}, \tag{18}$$

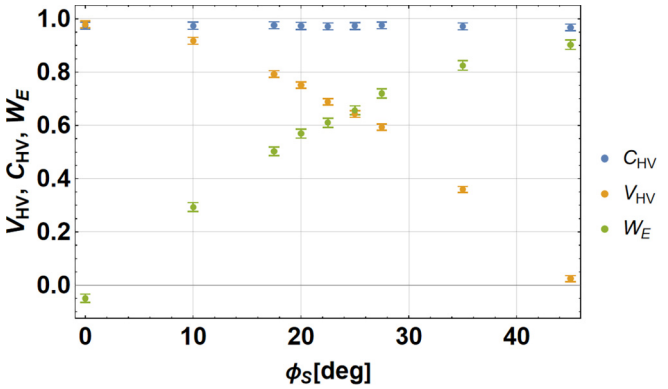

FIG. 2. Trade-off relation between the local polarization V_{HV} (yellow dots) and the entanglement witness W_E (green dots) controlled by the parameter ϕ_S. The blue dots show the correlation C_{HV} of HV polarization. As expected, ϕ_S controls the degree of entanglement without changing the correlation C_{HV}. See the Appendix for the raw data obtained in the experiment.

where N_H and N_V are the count rates of H polarization and V polarization for a single photon. Since the count rates can be different for the two photons, we obtained the average visibility V_{HV} for both outputs. The relation between the local polarization visibility V_{HV} and the entanglement witness W_E is given by the inequality

$$\sqrt{V_{HV}^2 + W_E^2} \leqslant 1. \tag{19}$$

The limit of 1 is obtained by the ideal state given in Eq. (10). It is therefore possible to quantify errors in the state preparation process by evaluating the length of the vector (V_{HV}, W_E). Similarly, the two photon visibility C_{HV} of the ideal state is always one. We can thus define two measures that evaluate the performance of our entanglement source.

Figure 2 shows the experimental results obtained for V_{HV}, C_{HV}, and W_E. The values of C_{HV} are consistent with the result obtained at $\phi_S = 45°$. At $\phi_S = 0°$, the local polarization is maximally defined and V_{HV} is approximately equal to C_{HV}. On the other hand, W_E is limited by the visibility of DA correlations, and these depend on quality of interference at the output of the Sagnac interferometer. Therefore, W_E stays below the value of C_{HV} at $\phi_S = 45°$, corresponding to the difference between the HV and the DA visibilities in Eqs. (15) and (16). For intermediate values of ϕ_S, Fig. 2 shows the trade-off relation between the local polarization V_{HV} and the entanglement witness W_E, where ϕ_S controls the degree of entanglement as theoretically predicted. The precise numerical values obtained in the experiment are shown in Table I. In addition, the values of $(V_{HV}^2 + W_E^2)^{1/2}$ are shown to indicate how close the experimental result is to the ideal state. Varying ϕ_S changes the balance between the HH and VV components in Eq. (10), resulting in an increase of entanglement as the balance approaches equality at $\phi_S = 45°$. The total amount of coherence in the emitted state is given by $(V_{HV}^2 + W_E^2)^{1/2}$, indicating the trade-off between local polarization V_{HV} and entanglement W_E. The reason why $(V_{HV}^2 + W_E^2)^{1/2}$ shows a slight but significant reduction as ϕ_S increases is that the entanglement described by W_E is generated by the interference effects at the output of the Sagnac interferometer, making W_E sensitive to mode matching errors at the DBPS. As expected, $(V_{HV}^2 + W_E^2)^{1/2}$ is equal to V_{HV} at $\phi_S = 0°$ and equal to W_E at $\phi_S = 45°$. The value of $(V_{HV}^2 + W_E^2)^{1/2}$ thus drops as the relative contribution of W_E increases.

IV. OPTIMIZATION OF CONTEXTUAL STATISTICS BY ADAPTIVE INPUT STATE CONTROL

A. Suppression of probabilities by local polarization rotations

As explained in Sec. II, the probabilities $P(0, a)$ $[P(a, 0)]$ can be suppressed by destructive quantum interferences between the components $|00\rangle$ and $|01\rangle$ ($|10\rangle$). Making use of the initial quantum coherence provided by the entanglement source, the suppression can thus be optimized by searching for the polarization rotation angles ϕ_M with equal probabilities for the outcomes (0,0) and (0,1). Due to the symmetry of the state generated by the entanglement source, we can assume that $P(0, 1) \approx P(1, 0)$, so that the same rotation angle ϕ_M can be used for both photons. A single rotation angle ϕ_M simultaneously minimizes both $P(0, a)$ and $P(a, 0)$, as can be verified after the determination of ϕ_M by directly measuring the residual probabilities of these outcomes.

To determine the optimal value of ϕ_M for a specific value of ϕ_S, we measured the coincidence counts of the outcome (0,0) or (0,1) at three different values of ϕ_M close to the theoretically expected value for that setting of ϕ_S. Since the dependence of the coincidence counts on ϕ_M is approximately linear in that region, three settings of ϕ_M are sufficient to identify the optimal value of ϕ_M, where the probabilities of

TABLE I. Experimental values of C_{HV}, V_{HV}, W_E, and $(V_{HV}^2 + W_E^2)^{1/2}$ for different settings of the parameter ϕ_S, including statistical error margins. The results characterize the control of entanglement by the experimental parameter ϕ_S.

ϕ_S [deg]	C_{HV}	V_{HV}	W_E	$\sqrt{V_{HV}^2 + W_E^2}$
0	0.975 ± 0.013	0.979 ± 0.013	−0.049 ± 0.016	0.980 ± 0.013
10	0.974 ± 0.013	0.918 ± 0.013	0.294 ± 0.017	0.963 ± 0.014
17.5	0.976 ± 0.013	0.793 ± 0.013	0.503 ± 0.017	0.938 ± 0.014
20	0.973 ± 0.013	0.751 ± 0.012	0.569 ± 0.017	0.943 ± 0.014
22.5	0.971 ± 0.013	0.689 ± 0.012	0.610 ± 0.017	0.920 ± 0.015
25	0.973 ± 0.013	0.642 ± 0.012	0.656 ± 0.017	0.918 ± 0.015
27.5	0.975 ± 0.013	0.594 ± 0.012	0.720 ± 0.017	0.933 ± 0.015
35	0.971 ± 0.013	0.359 ± 0.011	0.825 ± 0.018	0.900 ± 0.017
45	0.968 ± 0.013	0.025 ± 0.011	0.903 ± 0.018	0.903 ± 0.018

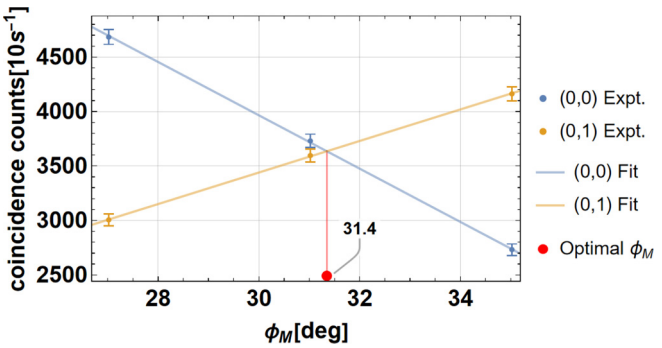

FIG. 3. Determination of the optimal value of ϕ_M for $\phi_S = 22.5°$. Count rates are obtained for the outcomes (0,0) and (0,1) at three different settings of ϕ_M. The optimal value of ϕ_M is found at the intersection of the lines representing the linear dependence of the count rates on ϕ_M. For $\phi_S = 22.5°$, the optimal value is found at $\phi_M = 31.4°$. Data were taken for three different angles ϕ_M, with one count rate for the (0,0) setting [(0,0) Expt] and one count rate for the (0,1) setting [(0,1) Expt]. The optimal value of ϕ_M for the subsequent experiments (optimal ϕ_M) is found by taking the intersection of the linear fits of the two sets of data points.

$P(0, 0)$ and $P(0, 1)$ are approximately equal. Figure 3 illustrates this method of finding the optimal values of ϕ_M for the case of $\phi_S = 22.5°$. The procedure is relatively simple and can be used to quickly identify the optimal local polarization rotation ϕ_M for several different degrees of entanglement. Table II shows the results we obtained for nine different values between $\phi_S = 0°$ and $\phi_S = 45°$.

The success of the suppression of probabilities for $P(a, 0)$ and $P(0, a)$ can be confirmed by measuring the corresponding detection probabilities at the optimal settings of ϕ_M. The results are shown in Table III. The probabilities given in the table are determined directly from the number of counts observed in a specific time interval, where the total count rate is determined by adding the four settings that correspond to a complete measurement basis. For example, the probability of $(a, 0)$ is given by

$$P(0, a) = \frac{N(0, a)}{N(0, a) + N(0, b) + N(1, a) + N(1, b)}. \quad (20)$$

TABLE II. Values of the optimal polarization rotation ϕ_M determined for different settings of the parameter ϕ_S. The numbers given are the settings used in the actual experiments, so they represent experimental parameters rather than experimental results.

ϕ_S [deg]	ϕ_M [deg]
0	46.3
10	38.8
17.5	33.7
20	32.7
22.5	31.4
25	30.5
27.5	29.5
35	26.7
45	22.2

TABLE III. Values of $P(0, a)$ and $P(a, 0)$ achieved by using the optimized values of ϕ_M. The value of $\frac{1}{4}(1 - C_{\mathrm{HV}})$ is also given since it may be the main source of the errors that limit the suppression of $P(0, a)$ and $P(a, 0)$ by the optimization of ϕ_M.

ϕ_S [deg]	$P(0, a)$	$P(a, 0)$	$\frac{1}{4}(1 - C_{\mathrm{HV}})$
0	0.0072 ± 0.0008	0.0030 ± 0.0005	0.0063 ± 0.0033
10	0.0078 ± 0.0008	0.0088 ± 0.0009	0.0065 ± 0.0033
17.5	0.0110 ± 0.0010	0.0070 ± 0.0008	0.0060 ± 0.0033
20	0.0100 ± 0.0009	0.0071 ± 0.0008	0.0067 ± 0.0033
22.5	0.0104 ± 0.0010	0.0062 ± 0.0007	0.0071 ± 0.0033
25	0.0125 ± 0.0010	0.0086 ± 0.0009	0.0068 ± 0.0033
27.5	0.0111 ± 0.0010	0.0080 ± 0.0008	0.0062 ± 0.0032
35	0.0137 ± 0.0011	0.0088 ± 0.0009	0.0071 ± 0.0032
45	0.0104 ± 0.0009	0.0097 ± 0.0009	0.0081 ± 0.0032

The statistical average of $P(0, a)$ and $P(a, 0)$ for the nine values of ϕ_S is 0.010 ± 0.002 and 0.007 ± 0.002, respectively, where the errors give the standard deviations for the distribution of values in the nine data points. Since the errors do not depend much on ϕ_S, we assume that they mostly originate from the errors in the correlation of the HV polarizations, C_{HV}. For a completely random state, $C_{\mathrm{HV}} = 0$ and $P(a, 0) = P(0, a) = 1/4$. Since the relations between probabilities and density-matrix elements are linear, we conclude that the error in $P(a, 0)$ and $P(0, a)$ caused by values of C_{HV} smaller than one is given by $(1 - C_{\mathrm{HV}})/4$. These values are shown in Table III alongside the values of $P(a, 0)$ and $P(0, a)$. The similarity in the magnitude of errors suggests that the residual probabilities of $P(a, 0)$ and $P(0, a)$ are an unavoidable consequence of the experimental imperfections that are also responsible for the errors in the correlations between the HV polarizations of the emitted photon pairs.

B. Evaluation of quantum contextuality

The purpose of adaptive state control is the observation of quantum contextuality. By suppressing the probabilities of the outcomes $(0, a)$, $(a, 0)$, and (1,1), we should obtain a much higher probability of the outcome (a, a), resulting in a clear violation of the inequality given in Eq. (4). This violation of noncontextual logic can be observed directly in the count rates of each of the outcomes. The raw data we obtained for the

TABLE IV. Experimentally observed counts obtained for the four outcomes $(0, a)$, $(a, 0)$, $(1, 1)$, and (a, a) in a ten second interval. Contextuality is confirmed when $N(a, a)$ is larger than the sum of the first three count rates.

ϕ_S [deg]	$N(0, a)$	$N(a, 0)$	$N(1, 1)$	$N(a, a)$
0	88	36	3354	40
10	88	95	954	304
17.5	125	79	231	752
20	113	79	155	959
22.5	118	71	172	1148
25	145	98	240	1357
27.5	136	97	285	1586
35	163	106	1002	2153
45	136	123	3513	3430

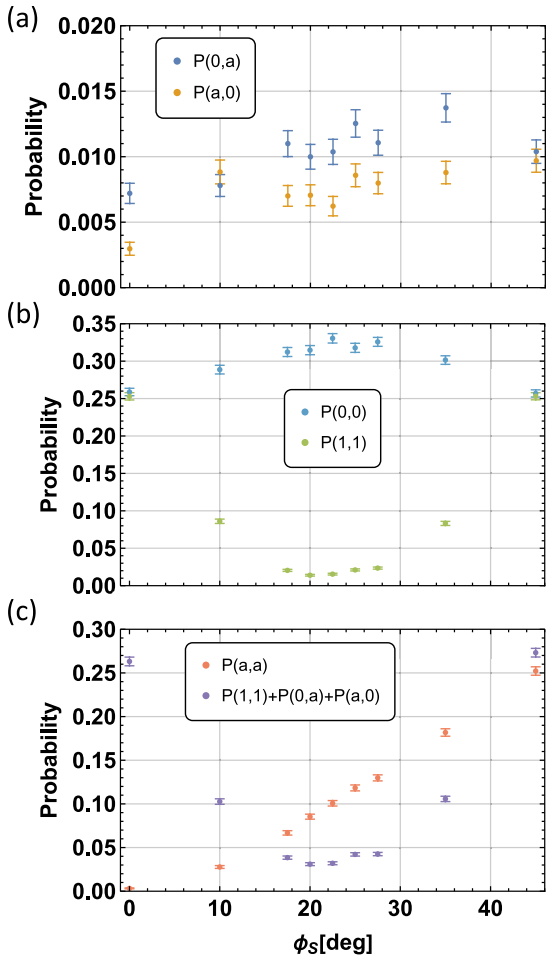

FIG. 4. Experimental results for the outcome probabilities $P(0,a)$, $P(a,0)$, $P(1,1)$, and $P(a,a)$ as a function of the parameter ϕ_S that determines the degree of entanglement. $\phi_S = 0^\circ$ is the separable case and $\phi_S = 45^\circ$ is the maximally entangled state. Panel (a) shows the results for the suppression of $P(0,a)$ and $P(a,0)$, panel (b) shows the results for the suppression of $P(1,1)$ in comparison with $P(0,0)$, and panel (c) shows the results for $P(a,a)$ and $P(0,a)+P(a,0)+P(1,1)$. Quantum contextuality is observed when $P(a,a)$ is larger than the sum of the three suppressed probabilities. See the Appendix for the raw data obtained in the experiment.

different settings are shown in Table IV. The number of counts $N(a,a)$ is higher than the sum of the other three counts for all settings from $\phi_S = 17.5^\circ$ to $\phi_S = 35^\circ$. The variation of the degree of entanglement results in low counts in the outcome (1,1) with a minimum between $\phi_S = 20^\circ$ and $\phi_S = 22.5^\circ$. Figure 4 shows the corresponding probabilities. Figure 4(a) shows the suppression of $P(0,a)$ and $P(a,0)$ discussed previously. Values are close to 0.01 or one percent throughout, confirming the successful optimization of ϕ_M. The symmetry breaking of the quantum state creates a difference between $P(0,a)$ and $P(a,0)$. Figure 4(b) shows the suppression of $P(1,1)$ by intermediate values of ϕ_S. Note the parabolic profile of $P(1,1)$ around the minimum between $\phi_S = 20^\circ$ and $\phi_S = 22.5^\circ$. The probability $P(0,0)$ is shown for comparison. Since the optimization of ϕ_M required that $P(0,0)$, $P(0,1)$, and $P(1,0)$ are approximately equal, the increase of $P(0,0)$ is equal to about one third of the decrease in $P(1,1)$. Figure 5

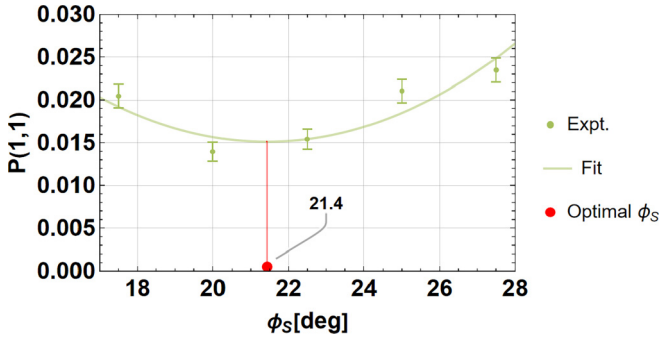

FIG. 5. Details of the results for $P(1,1)$ close to the minimum with a quadratic fit of the five points closest to the minimum. "Expt" indicates the experimental values, "Fit" indicates the quadratic fit, and "Optimal ϕ_S" indicates the value of ϕ_S at which the quadratic function of the fit is minimal. The minimum value of the fit is $P(1,1) = 0.0151 \pm 0.0016$ at $\phi_S = 21.4^\circ$.

shows the details of the minimum of $P(1,1)$ in Fig. 4(b), together with a quadratic fit of the data based on the five points closest to the minimum. Note that the minimum of the fit is slightly higher than the minimal experimentally determined value at $\phi_S = 20^\circ$, indicating that any setting of ϕ_S in the interval between 20° and 22.5° produces nearly indistinguishable results. The theoretical optimum obtained from the fit would be at $\phi_S = 21.4^\circ$, with a value of $P(1,1) = 0.0151 \pm 0.0016$ for the minimum. This result is consistent with the visibility in DA basis, as shown in Eq. (16). Finally, Fig. 4(c) illustrates the observation of quantum contextuality by comparing the probability $P(a,a)$ with the sum of the suppressed probabilities, $P(0,a) + P(a,0) + P(1,1)$. Due to the dependence of the suppression of $P(1,1)$ on ϕ_S, the sum of the suppressed probabilities has a minimum between $\phi_S = 20^\circ$ and $\phi_S = 22.5^\circ$. On the other hand, $P(a,a)$ increases monotonically with ϕ_S. As a result, quantum contextuality can be observed clearly at higher values of ϕ_S. Contextuality only disappears close to the maximally entangled state at $\phi_S = 45^\circ$.

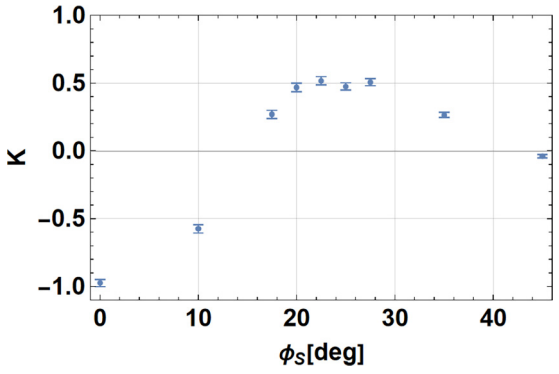

FIG. 6. Contrast function K determined from the experimental results using Eq. (21). A high value of the contrast function indicates the successful suppression of probabilities $P(0,a)$, $P(a,0)$, and $P(1,1)$, confirming the validity of the logical conditions set by the paradox. Negative values indicate that the inequality in Eq. (4) is not violated. The contrast K achieves a maximal value of about 0.5 in a wide region between $\phi_S = 20^\circ$ and $\phi_S = 27.5^\circ$, where the input state is defined by a nearly equal balance of local polarization and entanglement.

It may be interesting to consider the role of entanglement in the simultaneous suppression of the probabilities $P(0, a)$, $P(a, 0)$, and $P(1, 1)$, and in the subsequent observation of a nonzero value of $P(a, a)$. Figure 4(c) clearly shows that $P(a, a)$ increases together with the amount of entanglement characterized by the witness W_E. Since the maximal value of $P(a, a)$ is 0.25, this increase represents an increase in the randomness of the relation between the outcomes of $\{a, b\}$ measurements for the two photons. Local polarizations always prefer outcomes of b and therefore limit the probability $P(a, a)$. On the other hand, maximal entanglement makes it impossible to suppress $P(1, 1)$ together with $P(0, a)$ and $P(a, 0)$, since correlations between the outcomes of $\{0, 1\}$ measurements necessarily weaken the correlations between $\{0, 1\}$ and $\{a, b\}$. Optimal quantum contextuality is obtained when the suppression of $P(0, a)$ and $P(a, 0)$ is achieved by a combination of local polarization suppressing all a results and entanglement correlations suppressing the outcome combinations $(0, a)$ and $(1, b)$. This combination can apply simultaneously to a local suppression of 1 results and the combinations (1,1) and (0,0). Simultaneous suppression of all three outcomes $P(0, a)$, $P(a, 0)$, and $P(1, 1)$ can be achieved by both local polarization and entanglement, but only a balanced combination of both can achieve an optimal suppression effect. At the same time, suppression of a results by the local polarization will also limit the probability $P(a, a)$, adding an additional cost to the use of local polarization in the suppression of probabilities.

V. CONTRAST BETWEEN PROBABILITIES

The probability $P(1, 1)$ can only be suppressed by varying the entanglement of the input state. The lowest value of $P(1, 1)$ determined from the experimental data was obtained at $\phi_S = 20^\circ$ with $P(1, 1) = 0.0140 \pm 0.0011$. The data show a relatively flat minimum with very similar values of $P(1, 1)$ between $\phi_S = 20^\circ$ and $\phi_S = 22.5^\circ$. Moreover, the error rate is consistent with the two-photon visibilities C_{HV} and C_{DA} of the source. The sum of the suppressed probabilities at $\phi_S = 20^\circ$ is $P(0, a) + P(a, 0) + P(1, 1) = 0.0311 \pm 0.0016$. Experimental errors thus make it impossible to observe a probability of less than three percent in the suppressed probabilities. To observe quantum contextuality, it is therefore necessary to obtain a sufficiently high value of $P(a, a)$. At $\phi_S = 20^\circ$, this value is at $P(a, a) = 0.0854 \pm 0.0028$. However, higher values are obtained as ϕ_S increases. It is therefore desirable to evaluate the contrast between the low value of the probability sum $P(0, a) + P(a, 0) + P(1, 1)$ and the high value of the probability $P(a, a)$. This contrast can be defined as

$$K \equiv \frac{P(a, a) - P(0, a) - P(a, 0) - P(1, 1)}{P(a, a) + P(0, a) + P(a, 0) + P(1, 1)}. \tag{21}$$

By definition, the contrast K is one if and only if $P(0, a)$, $P(a, 0)$, and $P(1, 1)$ are all zero. If the probabilities do not violate the inequality in Eq. (4), K has a negative value. The value of K at $\phi_S = 20^\circ$ is $K = 0.467 \pm 0.032$, a clear violation of the inequality and a sufficiently clear contrast between the suppressed probabilities and the probability $P(a, a)$. However, the increase in $P(a, a)$ now results in slightly larger values of K for $\phi_S = 22.5^\circ$, $\phi_S = 25^\circ$, and even $\phi_S = 27.5^\circ$. The different values of K are shown in Fig. 6 and in Table V. The result clearly indicates that the observation of quantum contextuality is easier when the entanglement is larger than the entanglement of the ideal state defined by Eqs. (5)–(7).

TABLE V. Contrast K achieved at different settings of ϕ_S. Due to the low values of the probabilities compared by K, the errors are rather large. Values close to 0.5 are obtained for 20°, 22.5°, 25°, and 27.5°, indicating that the probability $P(a, a)$ is approximately three times as high as the sum of the three probabilities indicating a violation of the conditions required of the input state.

ϕ_S [deg]	K
0	-0.975 ± 0.026
10	-0.575 ± 0.031
17.5	0.269 ± 0.031
20	0.467 ± 0.032
22.5	0.518 ± 0.030
25	0.475 ± 0.027
27.5	0.506 ± 0.026
35	0.265 ± 0.019
45	-0.040 ± 0.013

As discussed before, the maximal value of the contrast K is obtained as the result of a trade-off between the contributions of local polarization and entanglement to the suppression of $P(1, 1)$ and the increase of $P(a, a)$. The condition imposed by the simultaneous suppression of $P(a, 0)$ and $P(0, a)$ limits the contribution of entanglement to the suppression of $P(1, 1)$, requiring a local suppression of the outcomes a. However, this local suppression of a also limits the probability $P(a, a)$. Adaptive input state control optimizes these relations in the presence of experimental imperfections, making optimal use of the available local polarization and the available entanglement. Although the contrasts that can be achieved are limited by the experimental imperfections, the range of parameters for which contrasts close to the maximum value can be obtained is much larger than the ideal case would seem to suggest. Adaptive input state control thus optimizes the robustness of quantum contextuality against experimental errors and decoherence.

VI. CONCLUSIONS

Quantum state preparation can be optimized to achieve maximal quantum contextuality in the presence of experimental imperfections. We achieve this by defining state preparation in terms of output probabilities that need to be minimized in order to observe quantum contextuality. In the present scenario, it was necessary to first determine the degree of entanglement of a two-photon state by setting a control parameter ϕ_S, followed by an optimization of local polarization rotations ϕ_M. Significantly, we were able to achieve a highly efficient optimization of ϕ_M by making use of the fact that quantum interference is maximal when the amplitudes of the interfering components are equal. Using this optimization method, we were then able to optimize the trade-off between entanglement and local polarization described by ϕ_S. The results show that the same contrast K between the probability of the paradoxical outcome (a, a) and the suppressed proba-

TABLE VI. Absolute counts in {H, V} or {D, A} basis for each ϕ_S. All counts were obtained in a 10-s interval.

ϕ_S [deg]	$N(H,H)$	$N(H,V)$	$N(V,H)$	$N(V,V)$	$N(D,D)$	$N(D,A)$	$N(A,D)$	$N(A,A)$
0	11326	119	27	47	3013	2926	2836	3033
10	10379	115	26	379	1895	3657	3611	1853
17.5	10030	107	28	1101	1369	4353	4387	1342
20	9860	111	40	1336	1152	4711	4506	1182
22.5	9391	109	51	1666	1082	4655	4640	969
25	9218	108	45	1947	946	4854	4935	895
27.5	9695	105	46	2415	767	5327	5464	812
35	7923	114	54	3689	459	5651	5611	430
45	5902	109	81	5611	207	5629	5795	175

bilities can be obtained for a wide range of different degrees of entanglement. This indicates that entanglement can partially compensate the effects of errors by increasing the probability of the outcomes (a, a). Importantly, adaptive state control allows us to directly optimize the statistics that characterize the actual input state, without any theoretical assumptions about the quantum coherence of the source.

As mentioned in the introduction, adaptive input state control has three distinct advantages: (a) It allows us to partially compensate the effects of experimental imperfections by optimizing the parameters that control the state preparation process, improving the performance of noisy sources. (b) It allows us to directly relate quantum state preparation to specific correlations relevant for the observation of contextuality paradoxes or similar purposes. (c) The optimization of quantum interference effects can be realized by observing the output probabilities of the components that interfere with each other, providing a particularly simple method of optimizing quantum coherent effects.

In conclusion, adaptive input state control allows us to optimize the nonclassical properties of quantum states in the presence of experimental imperfections by directly implementing specific statistical correlations that are relevant for the intended effects. Adaptive input state control thus makes fundamental aspects of quantum systems more accessible and may facilitate their application in future quantum information technologies.

ACKNOWLEDGMENTS

This work was supported by JST SPRING, Grant No. JPMJSP2132.

APPENDIX: COMPLETE SET OF RAW DATA OBTAINED IN THE EXPERIMENT

In the following, we present the raw data obtained in the experiment. Table VI shows the counts obtained within a 10-s interval for the measurement results used in the calculation of C_{HV}, V_{HV}, and W_E as shown in Fig. 2; Table VII shows the counts obtained in a 10-s interval for all combinations of a/b and $0/1$.

TABLE VII. Absolute counts with respect to (F, F), (F, W), (W, F), and (W, W) for each ϕ_S. All counts were obtained in a 10-s interval.

ϕ_S [deg]	$N(0,0)$	$N(0,1)$	$N(1,0)$	$N(1,1)$	$N(0,a)$	$N(0,b)$	$N(1,a)$	$N(1,b)$
0	3431	2989	3484	3354	88	5933	81	6119
10	3201	3377	3556	954	88	6510	564	4120
17.5	3527	3560	3979	231	125	7071	1442	2727
20	3496	3465	3993	155	113	7114	1782	2299
22.5	3688	3638	3661	172	118	7240	2159	1862
25	3624	3573	3967	240	145	7293	2492	1635
27.5	3952	3917	3977	285	136	7723	2990	1440
35	3631	3609	3803	1002	163	7020	4105	584
45	3565	3394	3408	3513	136	6444	6401	114
ϕ_S [deg]	$N(a,0)$	$N(a,1)$	$N(b,0)$	$N(b,1)$	$N(a,a)$	$N(a,b)$	$N(b,a)$	$N(b,b)$
0	36	38	6223	5824	40	38	95	12072
10	95	417	6453	3788	304	144	292	10224
17.5	79	1353	7323	2519	752	608	774	9123
20	79	1616	7264	2237	959	756	870	8649
22.5	71	2086	7501	1748	1148	959	1098	8196
25	98	2380	7434	1511	1357	1112	1210	7791
27.5	97	2850	7842	1359	1586	1357	1579	7697
35	106	4083	7199	671	2153	1964	2037	5691
45	123	6317	6107	144	3430	3370	3318	3483

[1] J. S. Bell, On the problem of hidden variables in quantum mechanics, Rev. Mod. Phys. **38**, 447 (1966).

[2] S. Kochen and E. P. Specker, The problem of hidden variables in quantum mechanics, in *The Logico-Algebraic Approach to Quantum Mechanics*, The University of Western Ontario Series in Philosophy of Science, Vol. 5a (Springer, Dordrecht, 1975), pp. 293–328.

[3] A. Peres, Incompatible results of quantum measurements, Phys. Lett. A **151**, 107 (1990).

[4] N. D. Mermin, Simple unified form for the major no-hidden-variables theorems, Phys. Rev. Lett. **65**, 3373 (1990).

[5] N. D. Mermin, Hidden variables and the two theorems of John Bell, Rev. Mod. Phys. **65**, 803 (1993).

[6] A. Cabello, Experimentally testable state-independent quantum contextuality, Phys. Rev. Lett. **101**, 210401 (2008).

[7] A. A. Klyachko, M. A. Can, S. Binicioğlu, and A. S. Shumovsky, Simple test for hidden variables in spin-1 systems, Phys. Rev. Lett. **101**, 020403 (2008).

[8] G. Kirchmair, F. Zähringer, R. Gerritsma, M. Kleinmann, O. Gühne, A. Cabello, R. Blatt, and C. F. Roos, State-independent experimental test of quantum contextuality, Nature (London) **460**, 494 (2009).

[9] R. Lapkiewicz, P. Li, C. Schaeff, N. K. Langford, S. Ramelow, M. Wieśniak, and A. Zeilinger, Experimental non-classicality of an indivisible quantum system, Nature (London) **474**, 490 (2011).

[10] M. F. Pusey, Anomalous weak values are proofs of contextuality, Phys. Rev. Lett. **113**, 200401 (2014).

[11] F. Piacentini, A. Avella, M. P. Levi, R. Lussana, F. Villa, A. Tosi, F. Zappa, M. Gramegna, G. Brida, I. P. Degiovanni, and M. Genovese, Experiment investigating the connection between weak values and contextuality, Phys. Rev. Lett. **116**, 180401 (2016).

[12] M. Waegell, T. Denkmayr, H. Geppert, D. Ebner, T. Jenke, Y. Hasegawa, S. Sponar, J. Dressel, and J. Tollaksen, Confined contextuality in neutron interferometry: Observing the quantum pigeonhole effect, Phys. Rev. A **96**, 052131 (2017).

[13] A. Auffèves and P. Grangier, A generic model for quantum measurements, Entropy **21**, 904 (2019).

[14] C. Budroni, A. Cabello, O. Gühne, M. Kleinmann, and J.-Å. Larsson, Kochen-specker contextuality, Rev. Mod. Phys. **94**, 045007 (2022).

[15] A. Aspect, P. Grangier, and G. Roger, Experimental realization of Einstein-Podolsky-Rosen-Bohm *gedankenexperiment*: A new violation of Bell's inequalities, Phys. Rev. Lett. **49**, 91 (1982).

[16] Z. Y. Ou and L. Mandel, Violation of Bell's inequality and classical probability in a two-photon correlation experiment, Phys. Rev. Lett. **61**, 50 (1988).

[17] G. Weihs, T. Jennewein, C. Simon, H. Weinfurter, and A. Zeilinger, Violation of Bell's inequality under strict einstein locality conditions, Phys. Rev. Lett. **81**, 5039 (1998).

[18] H. Takesue and K. Inoue, Generation of polarization-entangled photon pairs and violation of Bell's inequality using spontaneous four-wave mixing in a fiber loop, Phys. Rev. A **70**, 031802(R) (2004).

[19] H. Sakai, T. Saito, T. Ikeda, K. Itoh, T. Kawabata, H. Kuboki, Y. Maeda, N. Matsui, C. Rangacharyulu, M. Sasano *et al.*, Spin correlations of strongly interacting massive fermion pairs as a test of Bell's inequality, Phys. Rev. Lett. **97**, 150405 (2006).

[20] M. Ansmann, H. Wang, R. C. Bialczak, M. Hofheinz, E. Lucero, M. Neeley, A. D. O'Connell, D. Sank, M. Weides, J. Wenner *et al.*, Violation of Bell's inequality in Josephson phase qubits, Nature (London) **461**, 504 (2009).

[21] T. Kuroda, T. Mano, N. Ha, H. Nakajima, H. Kumano, B. Urbaszek, M. Jo, M. Abbarchi, Y. Sakuma, K. Sakoda, I. Suemune, X. Marie, and T. Amand, Symmetric quantum dots as efficient sources of highly entangled photons: Violation of Bell's inequality without spectral and temporal filtering, Phys. Rev. B **88**, 041306(R) (2013).

[22] B. Hensen, H. Bernien, A. E. Dréau, A. Reiserer, N. Kalb, M. S. Blok, J. Ruitenberg, R. F. Vermeulen, R. N. Schouten, C. Abellán *et al.*, Loophole-free Bell inequality violation using electron spins separated by 1.3 kilometres, Nature (London) **526**, 682 (2015).

[23] C. Ballance, V. Schäfer, J. P. Home, D. Szwer, S. C. Webster, D. Allcock, N. M. Linke, T. Harty, D. Aude Craik, D. N. Stacey *et al.*, Hybrid quantum logic and a test of Bell's inequality using two different atomic isotopes, Nature (London) **528**, 384 (2015).

[24] M. Giustina, M. A. M. Versteegh, S. Wengerowsky, J. Handsteiner, A. Hochrainer, K. Phelan, F. Steinlechner, J. Kofler, J.-Å. Larsson, C. Abellán, W. Amaya, V. Pruneri, M. W. Mitchell, J. Beyer, T. Gerrits, A. E. Lita, L. K. Shalm, S. W. Nam, T. Scheidl, R. Ursin, B. Wittmann, and A. Zeilinger, Significant-loophole-free test of Bell's theorem with entangled photons, Phys. Rev. Lett. **115**, 250401 (2015).

[25] L. K. Shalm, E. Meyer-Scott, B. G. Christensen, P. Bierhorst, M. A. Wayne, M. J. Stevens, T. Gerrits, S. Glancy, D. R. Hamel, M. S. Allman *et al.*, Strong loophole-free test of local realism, Phys. Rev. Lett. **115**, 250402 (2015).

[26] B. Hensen, N. Kalb, M. Blok, A. Dréau, A. Reiserer, R. Vermeulen, R. Schouten, M. Markham, D. Twitchen, K. Goodenough *et al.*, Loophole-free Bell test using electron spins in diamond: Second experiment and additional analysis, Sci. Rep. **6**, 30289 (2016).

[27] J. Kofler, M. Giustina, J.-Å. Larsson, and M. W. Mitchell, Requirements for a loophole-free photonic Bell test using imperfect setting generators, Phys. Rev. A **93**, 032115 (2016).

[28] J. P. Dehollain, S. Simmons, J. T. Muhonen, R. Kalra, A. Laucht, F. Hudson, K. M. Itoh, D. N. Jamieson, J. C. McCallum, A. S. Dzurak *et al.*, Bell's inequality violation with spins in silicon, Nat. Nanotechnol. **11**, 242 (2016).

[29] K. D. Jöns, L. Schweickert, M. A. Versteegh, D. Dalacu, P. J. Poole, A. Gulinatti, A. Giudice, V. Zwiller, and M. E. Reimer, Bright nanoscale source of deterministic entangled photon pairs violating Bell's inequality, Sci. Rep. **7**, 1700 (2017).

[30] W. Rosenfeld, D. Burchardt, R. Garthoff, K. Redeker, N. Ortegel, M. Rau, and H. Weinfurter, Event-ready bell test using entangled atoms simultaneously closing detection and locality loopholes, Phys. Rev. Lett. **119**, 010402 (2017).

[31] B. B. T. Collaboration *et al.*, Challenging local realism with human choices, Nature (London) **557**, 212 (2018).

[32] M. Zopf, R. Keil, Y. Chen, J. Yang, D. Chen, F. Ding, and O. G. Schmidt, Entanglement swapping with semiconductor-generated photons violates Bell's inequality, Phys. Rev. Lett. **123**, 160502 (2019).

[33] Y. Zhong, H.-S. Chang, K. Satzinger, M.-H. Chou, A. Bienfait, C. Conner, É. Dumur, J. Grebel, G. Peairs, R. Povey *et al.*,

Violating Bell's inequality with remotely connected superconducting qubits, Nat. Phys. **15**, 741 (2019).

[34] Z.-H. Liu, H.-X. Meng, Z.-P. Xu, J. Zhou, S. Ye, Q. Li, K. Sun, H.-Y. Su, A. Cabello, J.-L. Chen *et al.*, Experimental observation of quantum contextuality beyond Bell nonlocality, Phys. Rev. A **100**, 042118 (2019).

[35] D. Paneru, A. Te'eni, B. Y. Peled, J. Hubble, Y. Zhang, A. Carmi, E. Cohen, and E. Karimi, Experimental tests of multiplicative Bell inequalities and the fundamental role of local correlations, Phys. Rev. Res. **3**, L012025 (2021).

[36] D. Qu, K. Wang, L. Xiao, X. Zhan, and P. Xue, State-independent test of quantum contextuality with either single photons or coherent light, npj Quantum Inf. **7**, 154 (2021).

[37] S. Ru, W. Tang, Y. Wang, F. Wang, P. Zhang, and F. Li, Verification of Kochen-Specker-type quantum contextuality with a single photon, Phys. Rev. A **105**, 012428 (2022).

[38] D. M. Greenberger, M. A. Horne, A. Shimony, and A. Zeilinger, Bell's theorem without inequalities, Am. J. Phys. **58**, 1131 (1990).

[39] J.-W. Pan, D. Bouwmeester, M. Daniell, H. Weinfurter, and A. Zeilinger, Experimental test of quantum nonlocality in three-photon Greenberger–Horne–Zeilinger entanglement, Nature (London) **403**, 515 (2000).

[40] L. Hardy, Quantum mechanics, local realistic theories, and lorentz-invariant realistic theories, Phys. Rev. Lett. **68**, 2981 (1992).

[41] L. Hardy, Nonlocality for two particles without inequalities for almost all entangled states, Phys. Rev. Lett. **71**, 1665 (1993).

[42] W. T. M. Irvine, J. F. Hodelin, C. Simon, and D. Bouwmeester, Realization of Hardy's thought experiment with photons, Phys. Rev. Lett. **95**, 030401 (2005).

[43] J. R. Torgerson, D. Branning, C. H. Monken, and L. Mandel, Experimental demonstration of the violation of local realism without Bell inequalities, Phys. Lett. A **204**, 323 (1995).

[44] D. Boschi, F. De Martini, and G. Di Giuseppe, Test of the violation of local realism in quantum mechanics without Bell inequalities, Phys. Lett. A **228**, 208 (1997).

[45] D. Boschi, S. Branca, F. De Martini, and L. Hardy, Ladder proof of nonlocality without inequalities: Theoretical and experimental results, Phys. Rev. Lett. **79**, 2755 (1997).

[46] P. H. Eberhard, Background level and counter efficiencies required for a loophole-free Einstein-Podolsky-Rosen experiment, Phys. Rev. A **47**, R747 (1993).

[47] D. Frauchiger and R. Renner, Quantum theory cannot consistently describe the use of itself, Nat. Commun. **9**, 3711 (2018).

[48] M. Proietti, A. Pickston, F. Graffitti, P. Barrow, D. Kundys, C. Branciard, M. Ringbauer, and A. Fedrizzi, Experimental test of local observer independence, Sci. Adv. **5**, eaaw9832 (2019).

[49] M. Ji and H. F. Hofmann, Characterization of the nonclassical relation between measurement outcomes represented by nonorthogonal quantum states, Phys. Rev. A **107**, 022208 (2023).

[50] B.-S. Shi and A. Tomita, Generation of a pulsed polarization entangled photon pair using a Sagnac interferometer, Phys. Rev. A **69**, 013803 (2004).

[51] T. Kim, M. Fiorentino, and F. N. C. Wong, Phase-stable source of polarization-entangled photons using a polarization Sagnac interferometer, Phys. Rev. A **73**, 012316 (2006).

[52] F. Wong, J. Shapiro, and T. Kim, Efficient generation of polarization-entangled photons in a nonlinear crystal, Laser Phys. **16**, 1517 (2006).

[53] S. M. Lee, H. Kim, M. Cha, and H. S. Moon, Polarization-entangled photon-pair source obtained via type-ii non-collinear spdc process with ppktp crystal, Opt. Express **24**, 2941 (2016).

[54] M. Ji and H. F. Hofmann, Quantitative relations between different measurement contexts, arXiv:2305.14873.